Prediction of mechanical response for 5000-series Aluminum alloy coupling visco-plastic self-consistent approach with finite element method

Prediction of mechanical response for 5000-Series aluminum alloy coupling visco-plastic self-consistent approach with finite element method

IOP Conf. Series: Journal of Physics: Conf. Series **1063** (2018) 012104 doi:10.1088/1742-6596/1063/1/012104

Prediction of mechanical response for 5000-Series aluminum alloy coupling visco-plastic self-consistent approach with finite element method

A Ruggiero[1], M Hörnqvist Colliander[2], A H S Iyer[2], N Bonora[1], D Gentile[1], G Iannitti[1] and G Testa[1]

[1]DICeM, University of Cassino and Southern Lazio, Via G. Di Biasio 43, Cassino 03043, Italy
[2]Department of Physics, Chalmers University of Technology, Gothenburg, Sweden

E-mail: a.ruggiero@unicas.it

Abstract. In the present work, a hybrid micro macro-approach was adopted to investigate the material behavior of the A5XXX-O object of the Benchmark 3 of Numisheet2018. Starting from the provided uniaxial stress-strain curve and in house microstructure measurements, a mean field approach, by using the VPSC7c code, was used to perform numerical experiments in order to derive the anisotropic macroscopic behavior of the aluminum alloy.

Then, at the macroscale, a constitutive model was built on coupling a non-quadratic yield surface function with a damage model developed in the framework of the continuum damage mechanics. Finally, by using MSC.Marc2017.1, finite element simulations of uniaxial and Nakajima bulging tests were performed with the purpose of obtaining the Fracture Forming Limit Curve for the aluminum alloy under investigation.

1. Introduction

Sheet metal forming is a challenging topic for process engineering. Choosing the correct set of process parameters is a crucial point in avoiding failure during forming and obtaining good mechanical properties of the formed sheet. Numerical simulations can be an effective tool in reducing times and costs of experimental campaigns provided a good description of the material behavior up to failure. Then, constitutive modeling is a crucial issue that significantly influences accurateness and reliability of numerical results. In the last decades, scholars devoted a lot of work in improving the description of the mechanical response of formed sheet in terms of both strength and damage behavior.

Regarding the strength, the main point concerns the anisotropic behavior of the sheet due to the forming process and both macro and micro-approaches have been extensively investigated. At the macroscale, several yield surface functions have been proposed [1–3] and, successively, developed over the years. At the microscale, both mean and full-field approaches have been successfully adopted to predict the global response starting from the properties of the constituent single-crystal grains and accounting for the microstructure evolution during the plastic deformation process. Even if these approaches have been successfully implemented in finite element method (FEM) codes, the large number of degrees of freedom required still limits the applicability of such calculations at pure scientific applications.

In this work, a hybrid approach was adopted to address the anisotropic sheet properties of the A5XXX-O, object of the Benchmark 3 of Numisheet2018. Starting from the provided uniaxial stress-strain curve and in house microstructure measurements, the VPSC7c code, based on the viscoplastic (VP) self-consistent (SC) theory [4], was used to perform numerical experiments in order to obtain the macroscopic mechanical behavior of the aluminum alloy and extract coefficients of the Yld2004-18p model [5].

Regarding the failure, in many cases, formed sheets fail after the strain localization that controls the damage process. To capture the failure, an appropriate description of the sheet deformation is needed. To unbalance the geometric and boundary symmetries that prevent localization, geometric imperfection are inserted into numerical models to mimic heterogeneities of real sheets (e.g. Marciniak–Kuczynski model [6]). However, in the present case, failure occurs just after the strain localization preventing the use of such strategies. Failures is strictly connected to damage process, then physical variability has to be linked to the damage model. Here, the Bonora's damage model [7, 8], developed in the framework proposed by Lemaitre [9] in the context of the continuum damage mechanics (CDM) was adopted. Physical heterogeneity was introduced assuming a statistical variability for one of the damage model coefficients.

Finally, the constitutive model was used in the FE code MSC.Marc2017.1 to simulate uniaxial and Nakajima bulging tests with the scope of obtaining the Fracture Forming Limit Curve (FLC) for the A5XXX-O under investigation.

2. Material and texture measures

The material under investigation is an A5XXX-O aluminum alloy. Two samples were provided by the benchmark committee (sheet 10 and 11), with dimensions 50.0 mm by 50.0 mm, 1.0 mm thick. Texture measures were performed by electron backscatter diffraction (EBSD) on both the sheets on the RD-TD plane. An area of 2.4 mm by 2.6 mm was mechanically polished. The ODFs were calculated with the Matlab tool MTex 4.3.1, using the harmonic method and an order of the series expansion equal to 28. The {100}, {110}, and {111} pole figures (PF) reported in figure 1 show the texture for the sheet 10. Very similar texture was measured for the sheet 11.

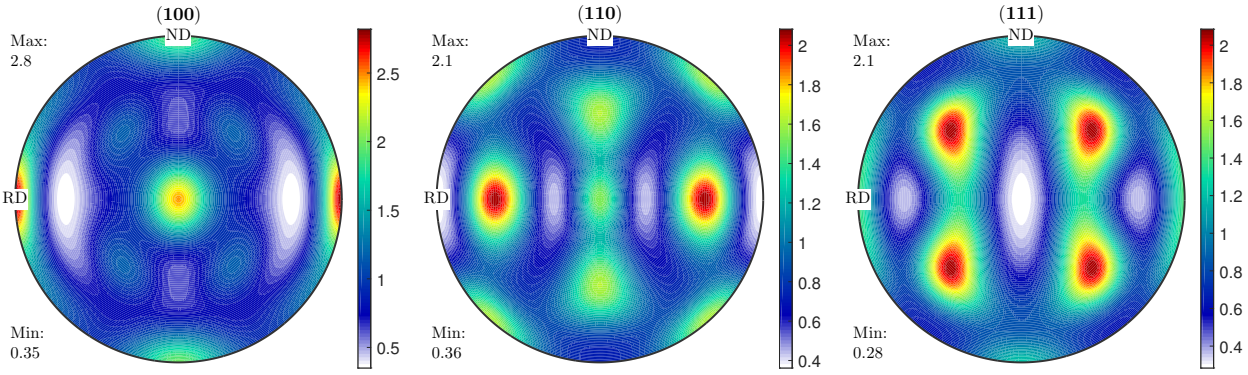

Figure 1. Pole figures of the measured texture (sheet 10).

3. Micromechanics analyses

Micromechanics analyses were performed with the code VPSC7c. The influence of neighboring grains was accounted for and the affine linearization method [10–12] was used at the grain level.

Slip hardening was modeled with the extended Voce curve [13].

$$\hat{\tau}^s = \tau_0^s + (\tau_1^s + \theta_1^s \Gamma)\left(1 - \exp\left(-\Gamma \left|\frac{\theta_0^s}{\tau_1^s}\right|\right)\right) \tag{1}$$

where $\Gamma = \sum_s \Delta\gamma^s$ is the accumulated shear in the grain; τ_0, θ_0, θ_1, $(\tau_0 + \tau_1)$ are the initial critical resolved shear stress (CRSS), the initial hardening rate, the asymptotic hardening rate and the back-extrapolated CRSS, respectively.

Coefficients were calibrated on the uniaxial stress-strain curve in the rolling direction (RD) provided for the Benchmark 3 of Numisheet 2018. Data obtained with a high resolution clip gauge, up to a strain of almost 0.1, were used. Since the aim of the work is to analyze the material behavior at high strains, the initial plateau was neglected. Analyses were performed using mixed boundary conditions: the velocity gradient components ($L_{ij} = \partial v_i/\partial x_j$) are given except for the two orthogonal directions to the tensile one for which the stress is imposed equal to zero . The calibrated coefficients of the slip work hardening are reported in table 1. Then, the calibrated model was used to perform a numerical experimental campaign to generate all data employed in section 4.1.

Table 1. Calibrated coefficient of the extended Voce curve describing the slip work hardening.

τ_0^s	τ_1^s	θ_0^s	θ_1^s
30.97	51.1	436.88	31.4

4. Macroscopic constitutive model

The macroscopic constitutive model is composed of three submodels: a yield surface, a hardening law, and a damage model. In the following the thee submodels are presented.

4.1. Yield surface

The Barlat's model [5], in the two forms Yld2004-13p and Yld2004-18p, was considered to describe the anisotropic behavior of the formed sheet. The calibrations of model coefficients were performed with the MSC.Marc tool "experimental data fit". As input the following data were used:

- the flow stresses and r-values in the uniaxial tension along 0°, 15°, 30°, 45°, 60°, 75°, and 90° from the RD;
- the equibiaxial r-value defined as the ratio $\dot{\varepsilon}_y/\dot{\varepsilon}_x$ obtained in the equibiaxial tensile test ($\sigma_x : \sigma_y = 1 : 1$);
- the biaxial flow stresses in the biaxial tension states with $\sigma_x : \sigma_y = 1 : -1$, $4 : 1$, $2 : 1$, $4 : 3$, $1 : 1$,

All data were obtained at the same value of plastic work W_0 calculated at $\varepsilon_0^p = 0.02$ in the uniaxial tensile test along the RD. According to Hosford (1972) and Logan and Hosford (1980), the exponent m was assumed to be equal to 8. All yield surfaces for zero shear are reported in figure 2. The comparison shows that neither of the two formulations is able to reproduce the stress state obtained with VPSC for $\sigma_x : \sigma_y = 4 : 1$ and $1 : 4$. However, the Yld2004-18p captures very well the other stress states and for this reason was the formulation selected for the finite element analyses. In figure 3 the Lankford coefficients obtained with the Yld2004-18p formulation are compared with the values obtained with VPSC7c.

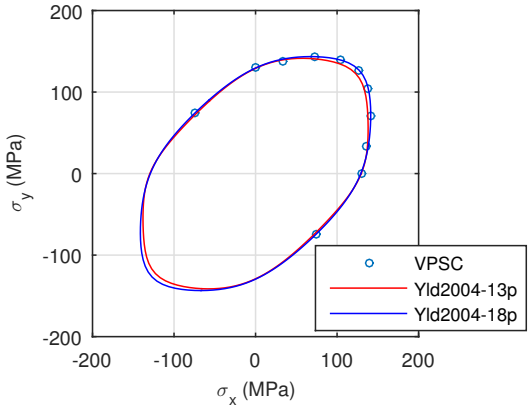

Figure 2. Yield surfaces.

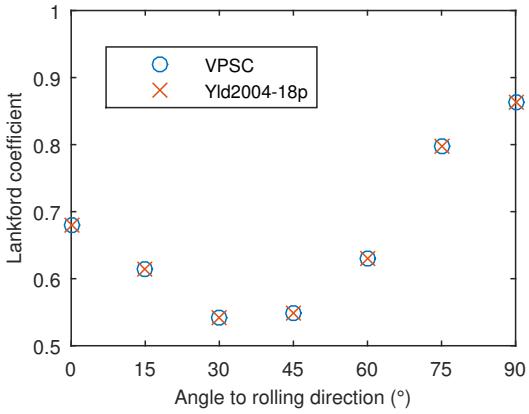

Figure 3. Lankford parameters.

4.2. Strength model

The extended form of the Voce law was used also to describe the macroscopic work hardening:

$$\sigma = \sigma_0 + (\sigma_1 + \beta_1 \varepsilon)\left(1 - \exp\left(-\varepsilon \left|\frac{\beta_0}{\sigma_1}\right|\right)\right) \tag{2}$$

the model coefficients, calibrated on the uniaxial true stress-logarithmic plastic strain curve in the RD, are given in table 2. The derivative of the calibrated curve, in figure 4, identifies the onset of necking at a plastic strain just before failure.

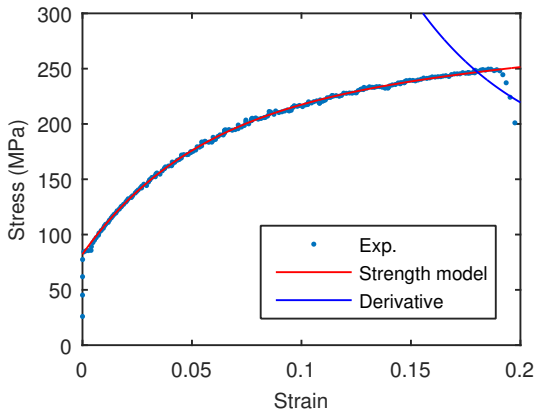

Figure 4. Uniaxial true stress-logarithmic plastic strain in the rolling direction in comparison with strength model curve and its derivative.

4.3. Damage model

To predict failure of the aluminum sheets, the Bonora's damage model [7, 8] was used. This, under the assumptions of isotropic damage and strain equivalence, relates the damage state variable to the effective elastic modulus of the material. The kinetic evolution law for the damage variable is given as follow:

$$\mathrm{d}D = \alpha \frac{D_{cr}{}^{\frac{1}{\alpha}}}{\ln\left(\varepsilon_f/\varepsilon_{th}\right)} R_\nu \left(D_{cr} - D\right)^{\frac{\alpha-1}{\alpha}} \frac{\mathrm{d}\varepsilon^+}{\varepsilon^+}, \tag{3}$$

The variable evolves with the total "active" equivalent plastic strain, ε^+, (i.e. the total equivalent plastic strain accumulated under tensile states of stress) and account for stress triaxiality, σ_H/σ_{eq}, according with the following relation:

$$R_\nu = \frac{2}{3}(1-\nu) + 3(1-2\nu)\left(\frac{\sigma_H}{\sigma_{eq}}\right)^2. \tag{4}$$

where ν is the Poisson's ratio, σ_H the hydrostatic stress, and σ_{eq} the von Mises stress.

The model, which results in a non linear damage accumulation with active plastic strain, requires the knowledge of four damage parameters, all having a physical meaning: the damage threshold strain, ε_{th}, at which damage processes initiates; the theoretical failure strain under constant uniaxial state of stress conditions, ε_f, at which ductile failure would occur; the critical damage, D_{cr}, at which failure occurs; and the damage exponent, α, that controls the shape of damage evolution with plastic strain. The parameters can be easily identified performing tensile tests on smooth and round notched specimen with axisymmetric [14, 15] or flat geometries [16]. Here, since data from round notched specimens were not available, the threshold strain was assumed, in first approximation, to be negligible. A very low value was assumed (0.002) since a null value cannot be handled by the model. Critical damage and α were chosen by referring to valid values for alloys of the same series, while ε_f and its standard deviation were calibrated on the experimental uniaxial stress-strain curve in the RD.

Table 2. Macroscopic strength model calibrated coefficients.

σ_0	σ_1	β_0	β_1
82.24	140.7	2804.46	158.6

Table 3. Bonora's damage model coefficients.

ε_{th}	ε_f	s_{ε_f}	D_{cr}	α
0.002	0.232	0.05	0.1	1.0

5. Uniaxial and biaxial test simulations

Numerical simulations were performed with the implicit FE commercial code MSC.Marc2017.1. Since the symmetries, for all configurations, a quarter of the specimen was model with eight-node, isoparametric, arbitrary hexahedral elements. Simulations were performed using large displacement, Lagrangian approach and finite strain formulation.

In figure 5 the calculated engineering stress-strain curve is compared with the experimental results. Failure strain and its standard deviation were calibrated on this curve in order to match the experimental results.

Then, the calibrated numerical model was used to simulate four different Nakajima test configurations. The full Nakajima test specimen and geometries with a parallel width of 43, 86, and 129 mm, all with notch radius of 107 mm. A 100 mm diameter hemispherical punch was adopted. The calculated FLC is reported in figure 6.

6. Conclusion

A hybrid micro macro-approach was used to investigate the material behavior of the A5XXX-O, object of the Benchmark 3 of Numisheet2018. The VPSC7c code, was employed to perform numerical experiments in order to derive the anisotropic macroscopic behavior of the material and extract coefficients of the Yld2004-18p model. Then, the yield surface was coupled to a damage model to predict, by virtual experiments, the aluminum alloy FLC. The approach resulted very effective in taking advantage of both the sophisticated capability of a mean field theory and the computational efficacy of a FE structural analysis.

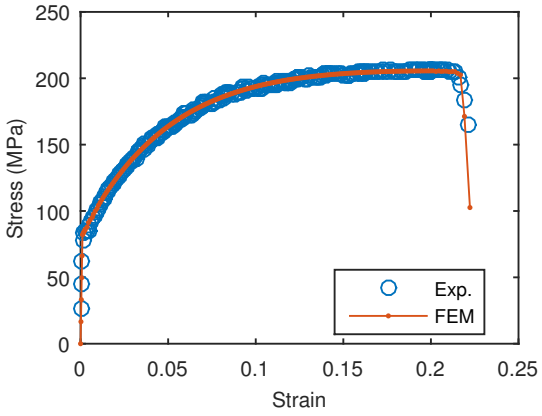

Figure 5. Engineering stress-strain curve in RD: comparison between experimental and FEM results.

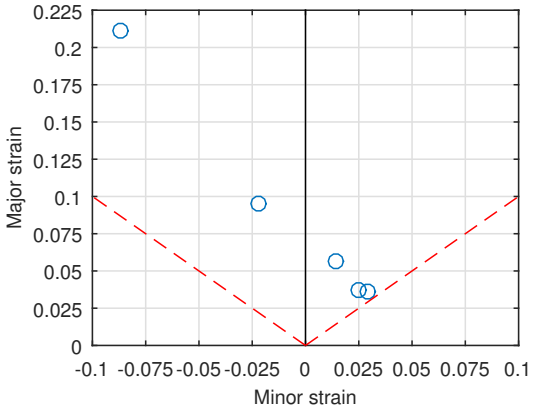

Figure 6. Calculated FLC for the A5XXX-O aluminum alloy.

Another point to underline is the introduction of statistical variability for one of the damage model coefficients. Considering the physical heterogeneity in the damage model rather than the geometry appears more effective, at least for this application, and has the advantage of correlating it directly to the material and not to the formed sheet.

References

[1] Hill R 1948 *Proc. R. Soc. London* A **193** 281
[2] Hosford W F 1972 *J. Appl. Mech.* **39** 607–9
[3] Barlat F, Lege D J and Brem J C 1991 *Int. J. Plast.* **7** 693–712
[4] Lebensohn R A and Tomé C N 1993 *Acta Metall. Mater.* **41** 2611–24
[5] Barlat F, Aretz H, Yoon J W, Karabin M E, Brem J C and Dick R E 2005 *Int. J. Plast.* **21** 1009–39
[6] Marciniak Z and Kuczyński K 1967 *Int. J. Mech. Sci.* **9** 609–20
[7] Bonora N 1997 *Eng. Fract. Mech.* **58** 11–28
[8] Bonora N, Ruggiero A, Esposito L and Gentile D 2006 *Int. J. Plast.* **22** 2015–47
[9] Lemaitre J 1985 *J. Eng. Mater. – T. ASME* **107** 83–9
[10] Masson R, Bornert M, Suquet P and Zaoui A 2000 *J. Mech. Phys. Solids* **48** 1203–27
[11] Lebensohn R A, Tomé C N and Maudlin P J 2003 *Los Alamos National Laborator Report*
[12] Lebensohn R A, Tomé C N and Maudlin P J 2004 *J. Mech. Phys. Solids* **52** 249–78
[13] Tomé C, Canova G R, Kocks U F, Christodoulou N and Jonas J J 1984 *Acta Metall.* **32** 1637–53
[14] Chiantoni G, Bonora N and Ruggiero A 2010 *Int. J. Mater. Form.* **3** 171–4
[15] Bonora N, Ruggiero A, Gentile D and De Meo S 2011 *Strain* **47** 241–54
[16] Majzoobi G H, Kashfi M, Bonora N, Iannitti G, Ruggiero A and Khademi E 2018 *Arch. Civ. Mech. Eng.* **18** 702–712